

Accepted Manuscript

Design, Manufacturing, and Testing of a Variable Stiffness Composite Cylinder

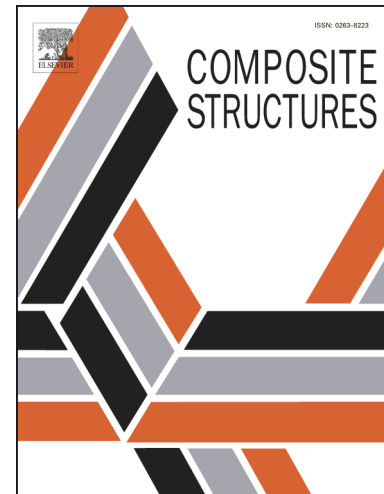
Mohammad Rouhi, Hossein Ghayoor, Jeffrey Fortin-Simpson, Tom T. Zacchia,
Suong V. Hoa, Mehdi Hojjati

PII: S0263-8223(17)32608-9

DOI: <https://doi.org/10.1016/j.compstruct.2017.09.090>

Reference: COST 8953

To appear in: *Composite Structures*



Please cite this article as: Rouhi, M., Ghayoor, H., Fortin-Simpson, J., Zacchia, T. T., Hoa, S. V., Hojjati, M., Design, Manufacturing, and Testing of a Variable Stiffness Composite Cylinder, *Composite Structures* (2017), doi: <https://doi.org/10.1016/j.compstruct.2017.09.090>

This is a PDF file of an unedited manuscript that has been accepted for publication. As a service to our customers we are providing this early version of the manuscript. The manuscript will undergo copyediting, typesetting, and review of the resulting proof before it is published in its final form. Please note that during the production process errors may be discovered which could affect the content, and all legal disclaimers that apply to the journal pertain.

Design, Manufacturing, and Testing of a Variable Stiffness Composite Cylinder

Mohammad Rouhi*, Hossein Ghayoor, Jeffrey Fortin-Simpson, Tom T. Zacchia,
Suong V. Hoa, Mehdi Hojjati

*Department of Mechanical and Industrial Engineering, Concordia Center for Composites,
Concordia University, Montreal, Quebec, Canada H3G 1M8*

Abstract

Fiber steering is one of the promising capabilities of Automated Fiber Placement (AFP) technology in manufacturing of advanced composite structures with spatially tailored properties. The so-called variable stiffness (VS) composites have considerable scope to outperform their traditionally made constant stiffness (CS) counterparts. However, there are several design and manufacturing challenges to be addressed before practically using them as structural components. In this work we demonstrate the design, manufacturing and testing procedure of a variable stiffness (VS) composite cylinder made by fiber steering. The improved bending-induced buckling performance is the objective of the VS cylinder to be compared with its CS counterpart. The experimental results show that the buckling capacity of the VS cylinder is about 18.5% higher than its CS counterpart.

Keywords:

Variable stiffness, Design optimization, Buckling, Composite manufacturing, Automated fiber placement

1. Introduction

Laminated fiber-reinforced composites are usually made by stacking plies with straight fibers and mostly limited to 0° , 90° , and $\pm 45^\circ$. Using straight fibers limits the tailorability of the composite structure to tailoring the stacking sequence of the laminate. This design space can be further extended by using curvilinear fibers in the

*Corresponding author: M. Rouhi,
Email address: m.rouhi@gmail.com

composite plies, e.g., allowing the plies to have continuously varying fiber orientation angles. Automated fiber placement (AFP) machines have made it possible to steer the fibers in individual plies to manufacture such laminates. The resulting variable stiffness (VS) laminate is capable of creating a more efficient load path between the loading points and the supports that allows harnessing the full potential of directional properties of composite materials. As a result, the VS composites made by fiber steering offer significantly improved performance compared with their constant stiffness (CS) counterparts [1, 2, 3, 4, 5, 6].

The most common manufacturing defects within fiber/tow steering are tow buckling, tow pull-up and tow misalignment [7]. Tow buckling occurs on the inside of the highly curved steering radius where the compressive force is too high. Likewise, tow pull-up may occur on the outside of highly curved steered fiber due to excessive tensile force. Tow misalignment can occur due to variability in the layup control or prepreg material. Tow gaps/laps are also other important steering-induced defects in VS composites of which the impact on the mechanical performance of the final products has not been extensively investigated.

The increased number of design variables introduces more challenges in the design optimization of VS composites such as modeling complexities and computational cost. Moreover, there are manufacturing issues associated with the VS composites to be taken into account such as gaps/overlaps, process efficiency, product quality, and manufacturability. Several review papers focused on different aspects of the VS composites potentials and challenges including the optimization methods [8], manufacturability [9], mechanical behavior of VS designs [10], and recently the maturity of VS designs [11]. The potential structural improvement that can be harnessed by fiber steering has been extensively studied [3, 12, 13, 14, 15, 16]. They all demonstrated that through stiffness tailoring, the loads are more efficiently redistributed that results in an optimum load path from the loading points to the supports. For a VS composite cylinder under bending-buckling load, Blom et al. [3, 17] predicted improvements of up to 17 percent compared to its baseline laminate. Khani et al. [12] showed that the buckling capacity of a VS cylinder can get about 24% higher than its CS counterpart. This improvement was about 21% for an elliptical cylinder. Rouhi et al. [18] showed that for elliptical cylinders under axial buckling there is about 118% improvement for VS over CS design. Ghayoor et al. [19] also investigated this potential improvement for bending-buckling of elliptical cylinders. Their results showed about 70% improvement in bending buckling of elliptical VS cylinders with cross-sectional aspect ratio of 0.7. Among several works reporting the potential improvement of composite structures' performance by fiber steering, a few of them have experimentally validated such improvements [3, 20, 21, 22]. Failure load of

composite flat panels with and without cutouts [20], and with large cutouts [21] were experimentally shown to be improved using fiber steering. Blom et al. [3] performed experimental testing for bending of a VS cylinder and compared their results with a QI baseline cylinder. They predicted the buckling improvement for VS cylinder, but did not go up to the buckling point to experimentally validate their prediction. White et al. [22] also performed axial buckling test and validated their results predicted by FEA in both buckling and post-buckling regions.

In this work a VS composite cylinder was designed and optimized for improved bending-induced buckling capacity over its CS counterpart which is a quasi-isotropic (QI) cylinder in this study. The experimental validation of the results for bending-buckling is performed for the first time. To this end, a multi-step metamodeling-based design optimization (MBDO) approach [23] combined with finite element analysis (FEA) were used. After finding the optimum fiber paths of the VS design, both QI and VS composite cylinders were manufactured by AFP machine and cured. The cylinders were thereafter prepared, installed on a bending machine and tested to assess their bending-buckling performance. The design, manufacturing, and testing procedures along with the experimental results were explained and discussed in details in the rest of this manuscript.

2. Modeling and Design Optimization

A composite cylinder with the gauge length and inside diameter of 381 mm was considered in this study. The material system of the composite plies were those of cured Carbon/Epoxy prepreg tows of which the mechanical properties of unidirectional layers are given in Table 1. The stacking sequence of $[\pm\theta/0/90]_s$ was considered in this study in which θ is kept unchanged and limited to 45° for QI cylinder, whereas for VS laminate it can vary in circumferential direction as shown in Fig. 1a.

The bending load is applied on the ends of the cylinder and the buckling load is computed by using the commercial FEA software ABAQUSTM. The FE model was generated using S8R5 shell elements and followed by a mesh convergence study, the cylinder was discretized into 100 points around the circumference. For the VS plies, the continuous variation of the fiber orientation angle in the circumferential direction was approximated by a piece-wise constant model in which the circumference is divided into a limited number (=100 in this study) of axial narrow bands with constant fiber orientation angles as shown in Fig. 1b. Therefore, stiffness tailoring was made by finding the orientation angle (θ_i) in each narrow band of the piece-wise constant model. To further reduce the number of the design variables, the orientation angles of certain equally-spaced narrow bands in each ply (T_i 's) are considered to be

Table 1: Material properties of each unidirectional carbon/epoxy composite ply (tow properties).

Property	Value
E_1 (GPa)	134
$E_2 = E_3$ (GPa)	7.71
$G_{12} = G_{13}$ (GPa)	4.31
G_{23} (GPa)	2.76
$\nu_{12} = \nu_{13}$	0.301
ν_{23}	0.396
V_f	0.55
Thickness (mm)	0.127

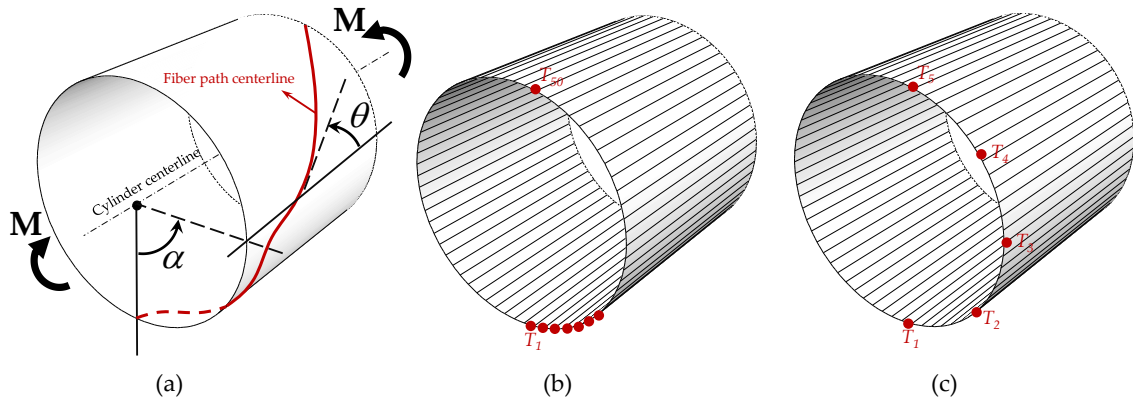


Figure 1: (a) Fiber path centerline for θ -plies in VS composite cylinder, (b) piece-wise constant approximation of varying orientation angle via discretization of the circumference, and (c) reducing the number of design variables.

the design variables (Fig. 1c). The orientation angles in other narrow bands were calculated by the linear interpolation between the design variables. Considering the symmetry about the vertical axis and the above mentioned definition of the design variables, 5 design variables were considered for a θ_i -ply to represent it as a VS lamina: T_1, \dots, T_5 . Therefore, the orientation angle of the k^{th} narrow band located between α_i and α_{i+1} is calculated by:

$$\theta_k = T_i + \frac{\alpha_k - \alpha_i}{\alpha_{i+1} - \alpha_i} (T_{i+1} - T_i) \quad i = 1, \dots, 5 \text{ and } k = 1, \dots, 10 \quad (1)$$

The effects of gaps/laps were not considered in this model and, as will be described in the manufacturing section in more details, the gauge length of the cylinders were manufactured so that there is no gap between the adjacent curvilinear tows but overlap was allowed.

Calculating the buckling load via FEA is computationally expensive. On the other hand, the design optimization usually is an iterative process that requires numerous function calls, i.e., FEA in this case. One way to overcome this problem is using a computationally efficient surrogate model on behalf of the FEA. Therefore, a metamodel-based design optimization (MBDO) was used for the VS cylinder. To reduce the error associated with the metamodeling and enhance the computational efficiency, a multi-step MBDO [23] was used in which the design domain is narrowed down step-by-step around the previously found optimum design point until the optimum design is converged.

The MBDO resulted in the optimum orientation angle distribution of VS plies as shown in Fig. 2. As observed, the tensile portion of the cylinder was stiffened because of small orientation angles of the fiber tows whereas the compressive portion was softened due to large orientation angles of the tows. As a result, the compressive load is partially transferred to the tensile part of the VS cylinder and the buckling capacity is expected to increase. The bending-buckling capacities of VS and QI cylinders calculated by FEA are listed in Table 2 in which the VS design shows about 28% improvement over its QI counterpart. The buckling mode shapes of the two cylinders were also shown in Fig. 3. It reveals that via stiffness tailoring the section loads are redistributed in a more efficient way. As a result, the compressive section load is partially transferred to the tensile part [3, 14, 15], a larger area in VS cylinder carries the compressive section load and the buckling capacity is improved.

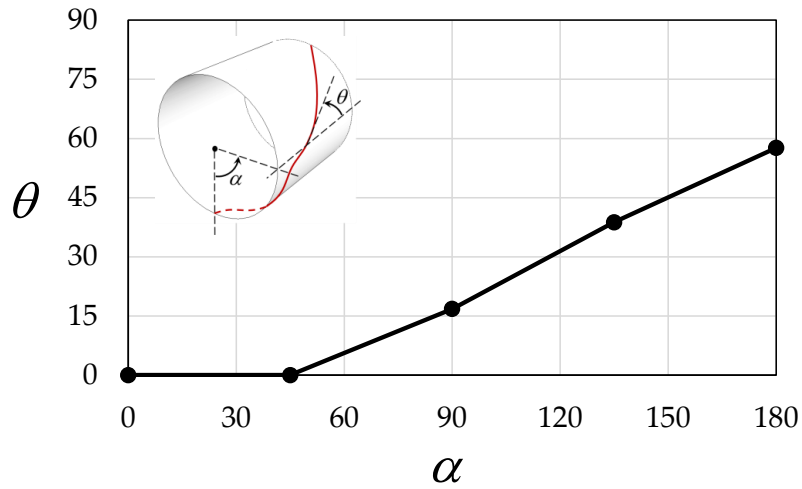


Figure 2: Circumferential orientation angle distribution of θ -plies in $[\pm\theta/0/90]_s$ stacking sequence.

Table 2: Bending buckling load of QI and VS composite cylinders.

Composite Cylinder	Buckling Load(kN.m)	Improvement(%)
Quasi-isotropic (QI)	20.7	–
Variable stiffness (VS)	26.6	28%

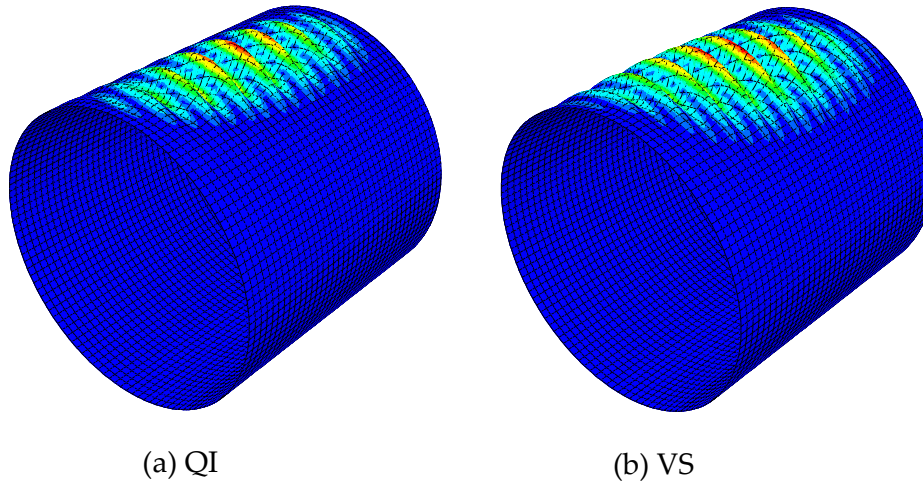


Figure 3: The bending-induced buckling mode shapes of (a) QI, and (b) VS cylinders.

3. Manufacturing and Experimental Setup for Testing

The orientation angle (OA) distribution over the circumference of VS plies was transformed to fiber paths using a finite difference method. Starting from any circumferential point at one end of the cylinder, any subsequent point of the tow path center line is determined by having the OA and a prescribed small differential distance from the preceding point. A spline passing through the resulted points from one end to the other end of the cylinder length defines the center line of each tow path. Therefore, starting from a different circumferential location results in a different path in a VS ply. The adjacent tow has to be placed so that there is no gap between the two tows in the gauge length of the cylinder (the middle 15-in long part). To this end, the starting point of the succeeding tow is calculated with the above mentioned constraint. Equation 2 shows how the gap distance is calculated between the two adjacent tows along the length of the cylinder:

$$GD = SD - \frac{TW}{2} \left(\frac{1}{\cos \theta_1} + \frac{1}{\cos \theta_2} \right) \quad (2)$$

where GD , SD , and TW are gap distance, shift distance and tow width, respectively, as shown in Fig. 4. The placement of a tow on the final path calculated via this method leaves a small gap with the first placed tow just before covering the whole surface of the cylinder in the gauge area of a VS ply. This gap is equally distributed between all the tows (distance between the starting points) to have the surface of the cylinder fully covered with negligible gap (less than 0.01 mm) between the adjacent tows at its gauge area.

The generated splines were converted to a commercial software SolidWorks (part) file readable by the AFP machine's computer console. The AFP machine placed the tows on a 1067-mm long steel mandrel with a diameter of 381 mm as shown in Fig. 5. To improve the tackiness between the tows and the substrate, the mandrel was pre-heated before the first ply tows were placed on the mandrel. The total length of the composite cylinder made by AFP was set to 762 mm: the 381-mm middle part as the gauge length and two 190.5-mm side parts to be held inside the bending assembly during the test. Following the fiber placement, the cylinder was vacuum-bagged and cured in the autoclave. Figure 6 shows the vacuum-bagged cylinder before and after curing. The bagging was then removed from the cured cylinder and the mandrel was extracted using the extraction machine seen in Fig. 7. This machine consists of a single drive motor that drives two ACME screws that are fixed to a connector which links to a shaft on the mandrel. The mandrel gets pulled into the machine while the part rests against a faceplate. It is worth noting that the mandrel was

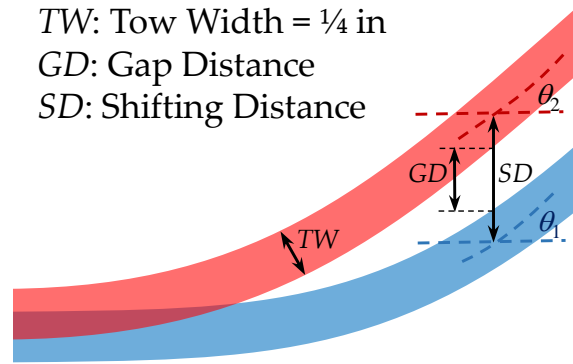


Figure 4: Gap distance between the adjacent steered tows through the length of the cylinder.

covered by releasing agent before fiber placement to facilitate the pull-out process of the cylinder. To assess the degree of cure, another small cylinder (dia.=247.6 mm) was made to go through the same curing cycle. Then small pieces from different parts of it were cut and tested by a differential scanning calorimeter (DSC) machine that showed the resin was fully cured. The void content of the cured cylinder was measured to be approximately 0.29% by cutting and visualization of the cross-section under scanning electron microscope (SEM).

As stated above, the two 190.5-mm side portions were strengthened by incrementally added tows making a ramp from the ends of the gauge length to the corrugated parts at the ends of the cylinder as shown in Fig. 8. The ramp was made to minimize the boundary effect in the bending test. The corrugated parts are placed inside the spaces provided in the two end rings of the bending assembly and surrounded by a low melting point alloy (LMPA). The solidification of the LMPA results in clamped supports for the cylinder at its two ends in the bending assembly as shown in Fig. 9. This was performed by preheating the assembly at each end, filling the space between the end rings with the liquefied LMPA, and letting it cool down to the room temperature. The two end plates of the assembly were also attached to each other with four braces to make sure the cylinder remains unloaded during handling and installation on the bending machine. The braces were removed from the assembly after its installation on the bending machine for testing.

Two data acquisition system were used to record the deformation of the cylinder during the loading: (1) strain gauges and (2) digital image correlation (DIC) system. Ten T-Rosette and one linear strain gauges were installed on the outer sur-

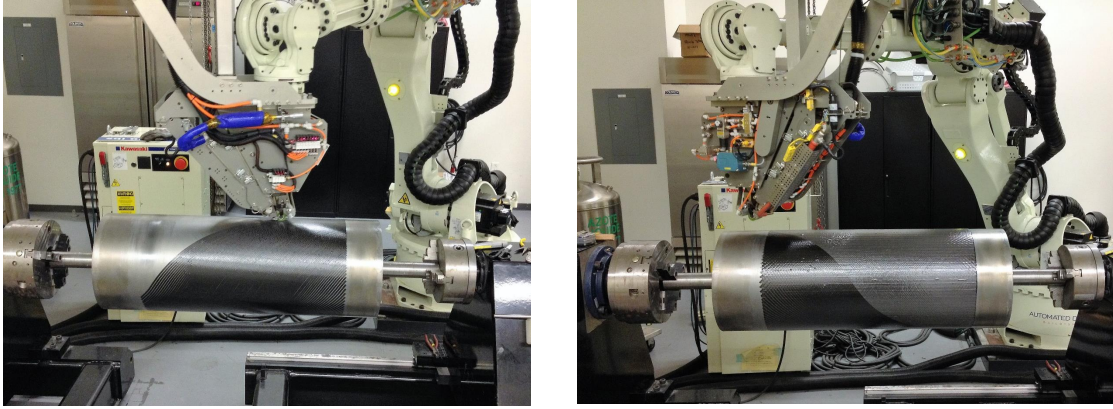


Figure 5: Fiber steering of the VS plies by AFP machine for a (a) θ -ply and (b) $-\theta$ -ply.

face of the cylinder to record strains during the test. The DIC cameras were also installed to measure the deformation of the cylinder during the loading. To this end, the outer surface of the cylinder was speckled with white markers as shown in Fig. 10.

The bending load was provided by two hydraulic cylinders connected to the ends of the two arms of the bending machine. The load cells on the hydraulic cylinders read the applied loads and the bending load was calculated by multiplying them to their arm lengths (571.5 mm). All of the measuring instruments were connected to a data acquisition system to record the load deformation data during the test.

4. Results and discussion

The structural performance of the VS cylinder in bending was assessed by plotting the bending moment in terms of (1) the axial strain at the bottom of the cylinders (Fig. 12) and (2) the bending rotation of the cylinders. It is worth noting that this rotation is about the horizontal radial line at mid length of the cylinder shown as γ in Fig. 13. The bending moment was calculated from taking the average values of the two hydraulic cylinders' load cells multiplied by their arm length (571.5 mm). The rotation of the cylinders were calculated from converting the linear displacement of the moving ends of the hydraulic cylinders measured by LVDT sensors into rotation. This approximation along with the small slippages in different parts of the machine results in less smooth plot of the moment-rotation (Fig. 13) compared to the moment-strain (Fig. 12). The overall behavior, however, is identical in both cases. As expected and observed, the VS cylinder is structurally stiffer in bending because



Figure 6: The AFP made cylinder was vacuum bagged for autoclave curing.

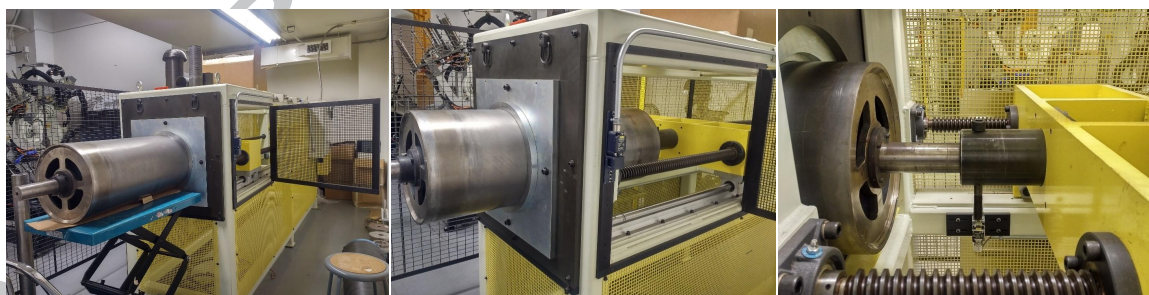


Figure 7: Cylinder removal machine for pulling out the cured cylinder from the mandrel.

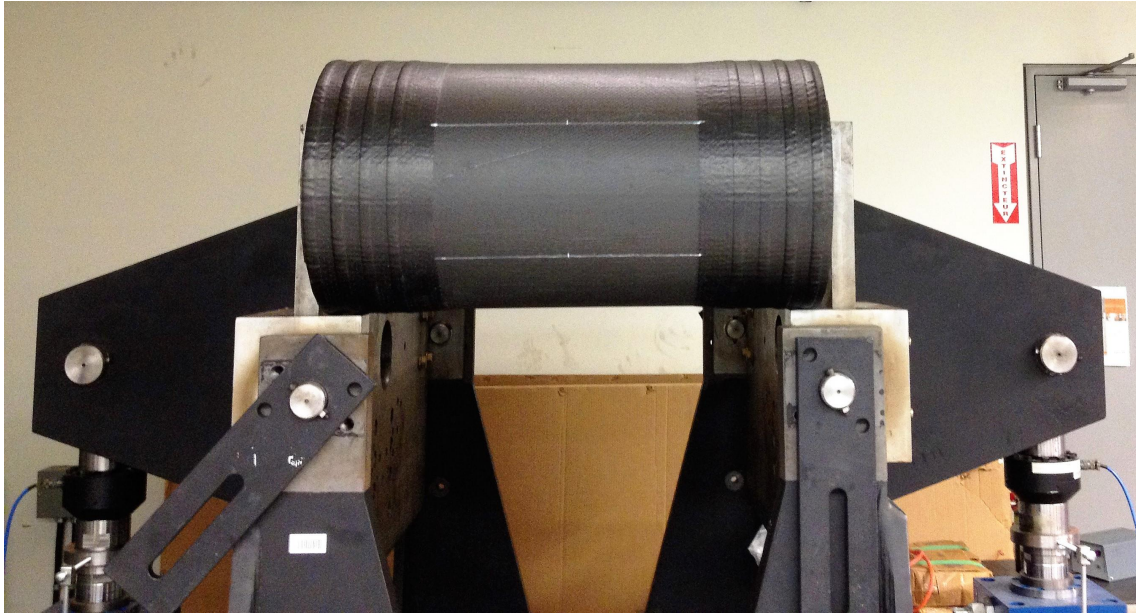


Figure 8: Composite cylinder made by AFP with strengthened ends (corrugated regions) in front of the bending machine before installation.

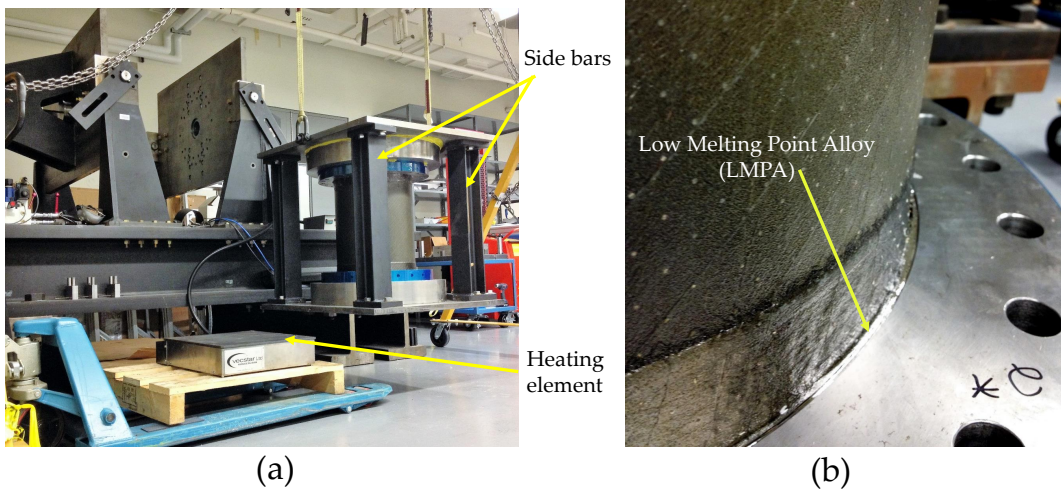


Figure 9: (a) Assembly with side bars to fix and install the cylinder on the bending machine, and (b) filling the ends of the cylinder's surrounding with LMPA to make clamped boundary conditions.

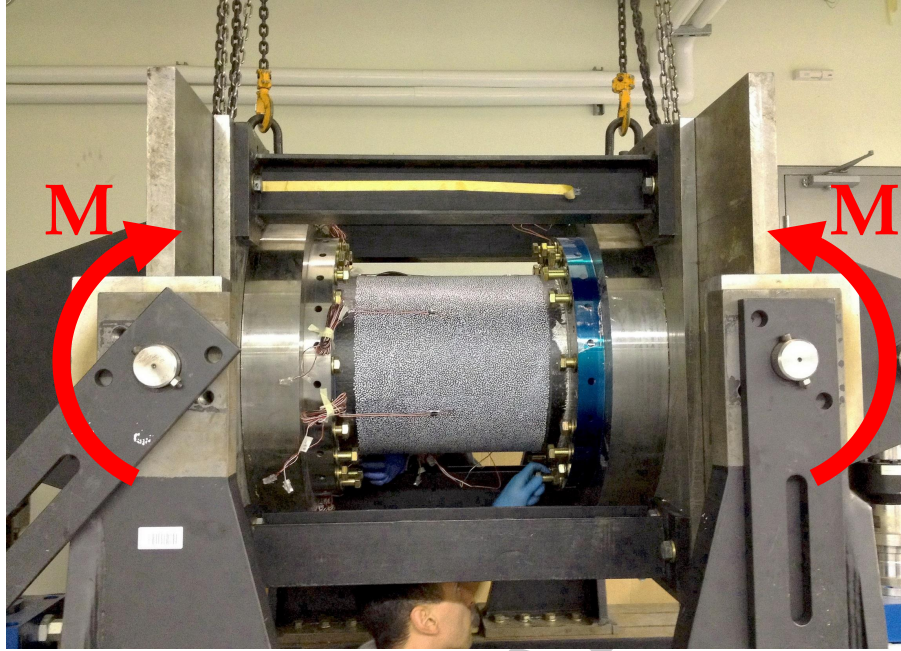


Figure 10: The composite cylinder being installed on the bending machine before removing the braces.

of the higher percentage of 0° -plies in the bottom portion of VS cylinder compared to its QI counterpart (see Fig. 2). The buckling load of the VS cylinder (22.06 kN.m) is also about 18.5% higher than the QI cylinder (18.6 kN.m). Compared to the FEA predictions in Table 2, the experimental results show about 17% and 10% lower-than-expected buckling loads for VS and QI cylinders, respectively. As a consequence, the experimental buckling improvement (18.5%) is about 9.5% lower than the theoretical value (28%). It shows that there are more manufacturing defects in the VS cylinder than the QI cylinder that unfavorably affect their structural performance. Figure 14 shows a close view of steered tows on the mandrel in which the small waviness occurs in those portion of the tows located inside the steering radius. This induced waviness results in additional reduced stiffness from the theoretical values considered in the design process for steered plies. Other manufacturing and processing defects, along with experimental errors are common for VS and QI cylinders that generally cause reduction in the predicted buckling capacity for both cylinders.

Figure 15 shows the circumferential distribution of the axial strains measured by the strain gauges installed on the two cylinders at 10 kN.m bending moment that is in the linear range before buckling occurs. Two important results revealed

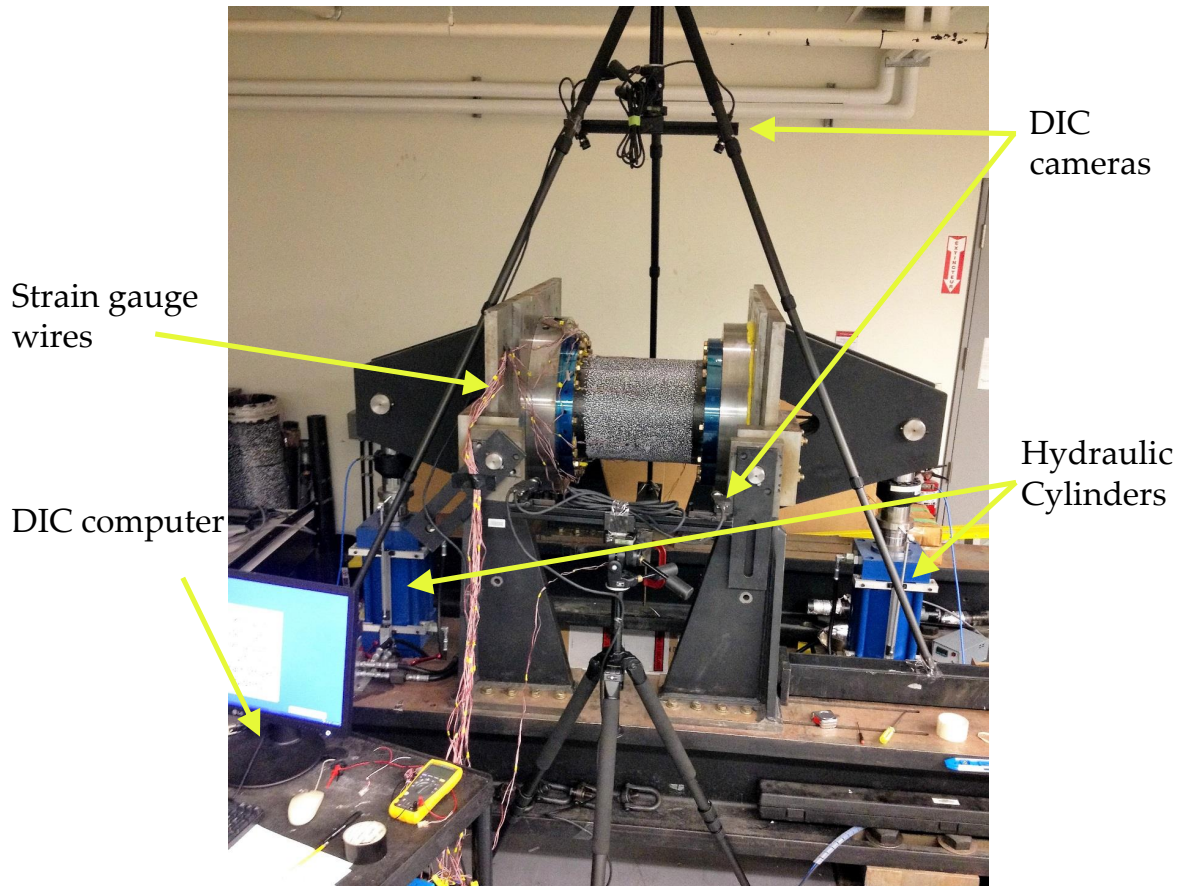


Figure 11: The composite cylinder installed on the bending machine with removed braces and ready for bending test.

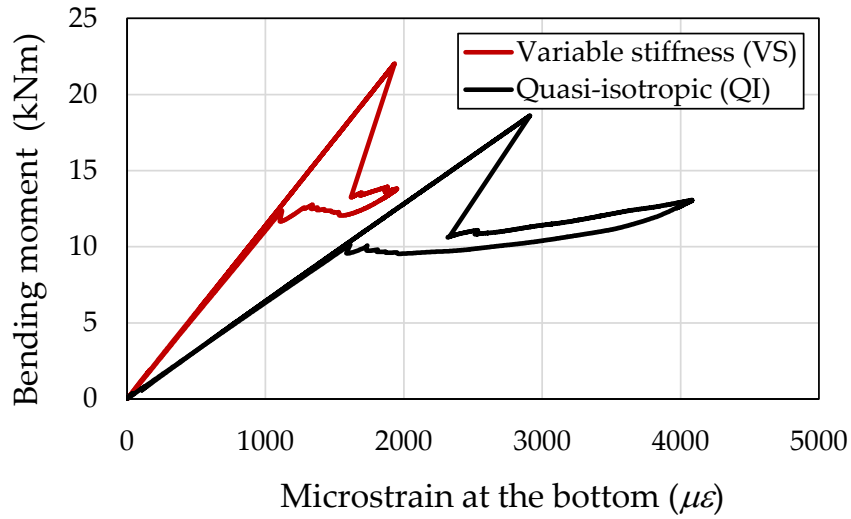


Figure 12: The bending moment in terms of the axial strain measured at the bottom (tension side) of the cylinders.

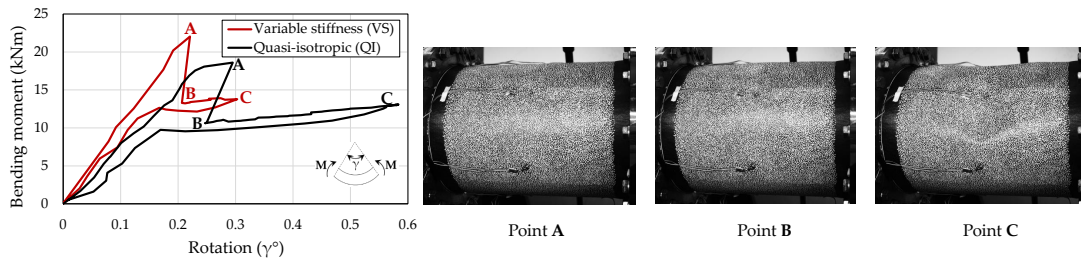


Figure 13: The bending moment in terms of the rotational deformation of the cylinders, and the front view of the cylinders at (A) buckling, (B) first localization right after buckling, and (C) deep postbuckling state.

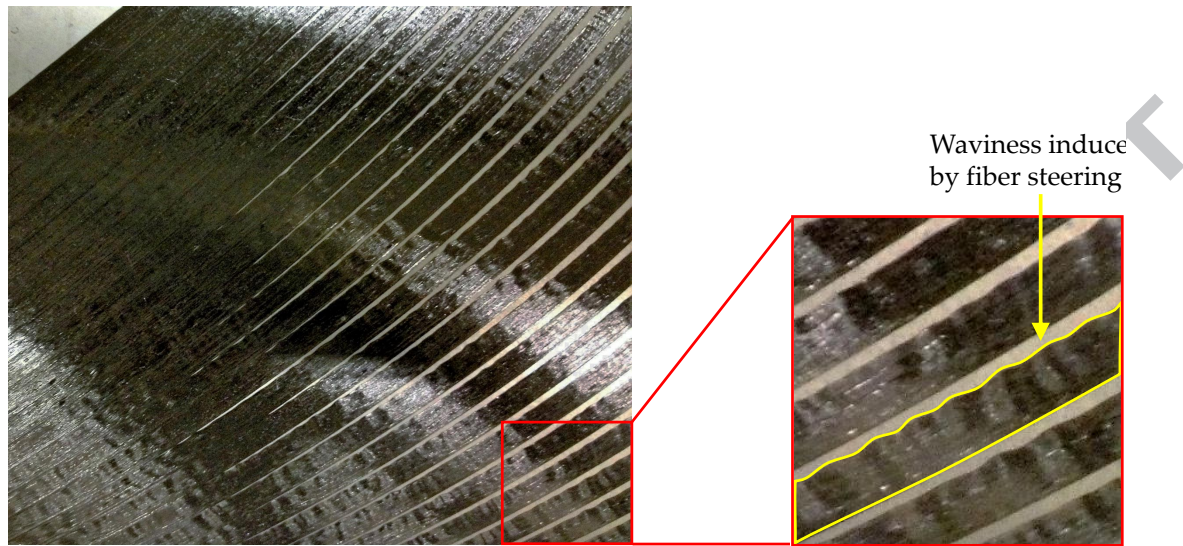


Figure 14: Waviness occurs at the inner radius of the steered tows.

by Fig. 15 are (1) the structural bending stiffness of VS cylinder was increased by fiber steering, and (2) the neutral axis was shifted from the middle ($\alpha = 90^\circ$ in QI) towards the tension side ($\alpha \approx 80^\circ$ in VS). This is due to the stiffness increase in the tension side and decrease in the compression side by fiber steering. As such, the proportion of material under compression is more in the VS cylinder compared to the QI cylinder. This is reflected in the mode shapes in Fig. 3. As a result, the directional properties of the composite were used more efficiently to redistribute the section load so that the tension side carried the tension load more effectively and, on the other hand, the compression load were carried by a larger portion of the cylinder.

Figure 16 shows the distribution of the axial strain on the surface of the QI and VS cylinders taken by the digital image correlation (DIC) cameras from the top of the cylinders. Similar buckling mode (first mode) was observed for the two cylinders at their respective buckling moments (Point A). In the VS cylinder, however, a relatively wider wavy area was observed showing a relatively larger area contributing in carrying the compressive load.

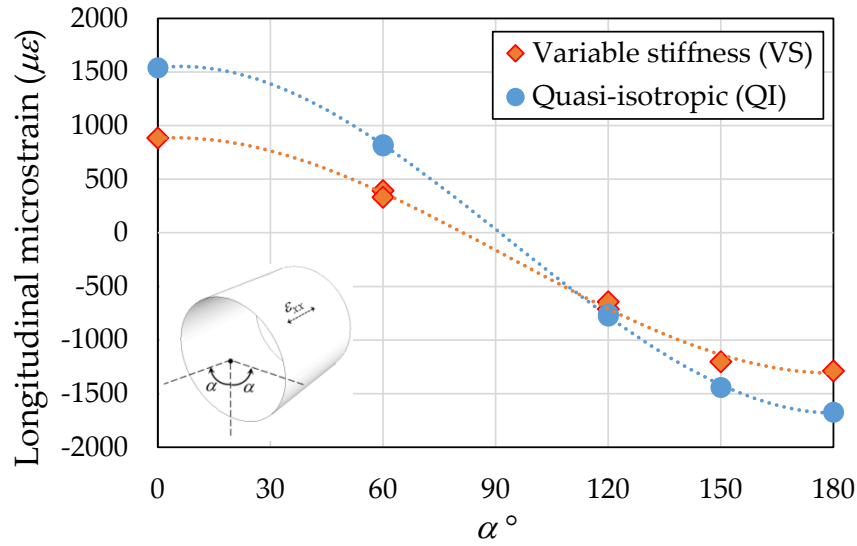


Figure 15: The distribution of the axial strain at $M=10$ kNm, measured by the strain gauges mounted on the circumference of the cylinders at the mid-length.

5. Concluding Remarks

The design optimization, manufacturing, and testing of a variable stiffness composite cylinder was performed. Via a surrogate-based modeling and design optimization method it was shown that the bending-buckling capacity of a QI cylinder can be improved about 28% by fiber steering of only 50% of the total plies. The designed VS and QI cylinders were manufactured by automated placement (AFP) machine and tested on a bending machine. The bending tests resulted in about 18.5% improvement in buckling load for VS cylinder compared to its QI counterpart. The manufacturing defects such as the steering-induced waviness of tows were shown in VS plies and thought to be the reason for the buckling improvement not reaching to its predicted value by theory. Yet, the improvement gained by the test was significant. It was also observed that the VS cylinder is structurally stiffer than its QI counterpart in bending.

Acknowledgement

The financial contributions from the Natural Sciences and Engineering Research Council of Canada (NSERC) industrial chair on Automated Composites, Bell Helicopter Textron Canada Ltd., Bombardier Aerospace, and Concordia University are

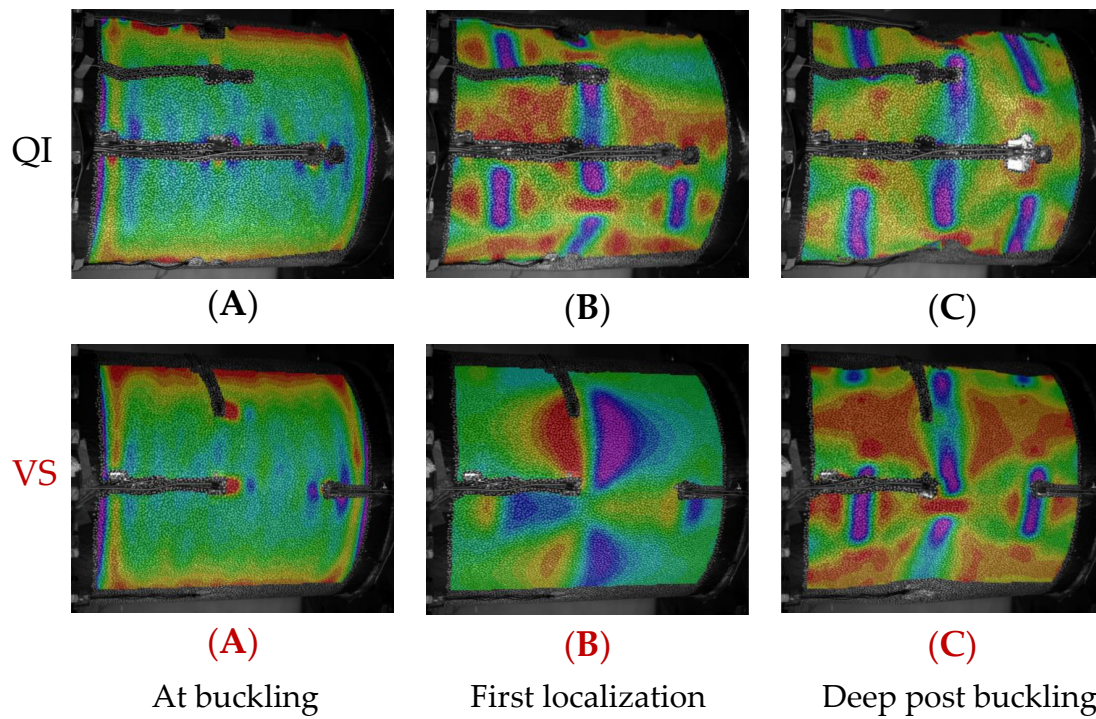


Figure 16: The axial strain distribution on the top (compression side) of the cylinders taken by the DIC camera system at (A) Buckling, (B) first localization, and (C) deep postbuckling.

appreciated.

ACCEPTED MANUSCRIPT

References

- [1] M. W. Hyer, R. F. Charette, Use of curvilinear fiber format in composite structure design, *AIAA J* 29 (6) (1991) 1011–1015.
- [2] A. W. Blom, B. F. Tatting, J. Hol, Z. Gürdal, Fiber path definitions for elastically tailored conical shells, *Compos Part B: Eng* 40 (1) (2009) 77–84.
- [3] A. W. Blom, P. B. Stickler, Z. Gürdal, Optimization of a composite cylinder under bending by tailoring stiffness properties in circumferential direction, *Compos Part B: Eng* 41 (2) (2010) 157–165.
- [4] M. Sun, M. Hyer, Use of material tailoring to improve buckling capacity of elliptical composite cylinders, *AIAA J* 46 (3) (2008) 770–782.
- [5] A. Alhajahmad, M. Abdalla, Z. Gürdal, Optimal design of tow-placed fuselage panels for maximum strength with buckling considerations, *J Aircr* 47 (3) (2010) 775–782.
- [6] J. Van Campen, C. Kassapoglou, Z. Gürdal, Generating realistic laminate fiber angle distributions for optimal variable stiffness laminates, *Compos Part B: Eng* 43 (2) (2012) 354–360.
- [7] D. H.-J. Lukaszewicz, C. Ward, K. D. Potter, The engineering aspects of automated prepreg layup: History, present and future, *Composites Part B: Engineering* 43 (3) (2012) 997–1009.
- [8] H. Ghiasi, K. Fayazbakhsh, D. Pasini, L. Lessard, Optimum stacking sequence design of composite materials part ii: Variable stiffness design, *Composite Structures* 93 (1) (2010) 1–13.
- [9] G. G. Lozano, A. Tiwari, C. Turner, S. Astwood, A review on design for manufacture of variable stiffness composite laminates, *Proceedings of the Institution of Mechanical Engineers, Part B: Journal of Engineering Manufacture* 230 (6) (2016) 981–992.
- [10] P. Ribeiro, H. Akhavan, A. Teter, J. Warmiński, A review on the mechanical behaviour of curvilinear fibre composite laminated panels, *Journal of Composite Materials* 48 (22) (2014) 2761–2777.
- [11] A. Sabido, L. Bahamonde, R. Harik, M. J. van Tooren, Maturity assessment of the laminate variable stiffness design process, *Composite Structures* 160 (2017) 804–812.

- [12] A. Khani, M. Abdalla, Z. Gürdal, Circumferential stiffness tailoring of general cross section cylinders for maximum buckling load with strength constraints, *Compos Struct* 94 (9) (2012) 2851–2860.
- [13] S. White, P. Weaver, Bend-free shells under uniform pressure with variable-angle tow derived anisotropy, *Compos Struct* 94 (11) (2012) 3207–3214.
- [14] M. Rouhi, H. Ghayoor, S. V. Hoa, M. Hojjati, Effect of structural parameters on design of variable-stiffness composite cylinders made by fiber steering, *Compos Struct* 118 (2014) 472–481.
- [15] M. Rouhi, H. Ghayoor, S. V. Hoa, M. Hojjati, Multi-objective design optimization of variable stiffness composite cylinders, *Composites Part B: Engineering* 69 (2015) 249–255.
- [16] M. Rouhi, H. Ghayoor, S. V. Hoa, M. Hojjati, The effect of the percentage of steered plies on the bending-induced buckling performance of a variable stiffness composite cylinder, *Science and Engineering of Composite Materials* 22 (2) (2015) 149–156.
- [17] A. W. Blom, Structural performance of fiber-placed variable-stiffness composite conical and cylindrical shells, Ph.D. thesis, Delft University of Technology (2010).
- [18] M. Rouhi, H. Ghayoor, S. V. Hoa, M. Hojjati, P. M. Weaver, Stiffness tailoring of elliptical composite cylinders for axial buckling performance, *Composite Structures* 150 (2016) 115 – 123.
- [19] H. Ghayoor, M. Rouhi, S. V. Hoa, M. Hojjati, Use of curvilinear fibers for improved bending-induced buckling capacity of elliptical composite cylinders, *International Journal of Solids and Structures* 109 (2017) 112 – 122.
- [20] C. S. Lopes, P. P. Camanho, Z. Gürdal, B. F. Tatting, Progressive failure analysis of tow-placed, variable-stiffness composite panels, *International Journal of Solids and Structures* 44 (25) (2007) 8493–8516.
- [21] A. Khani, M. Abdalla, Z. Gürdal, J. Sinke, A. Buitenhuis, M. V. Tooren, Design, manufacturing and testing of a fibre steered panel with a large cut-out, *Composite Structures*.

- [22] S. C. White, P. M. Weaver, K. C. Wu, Post-buckling analyses of variable-stiffness composite cylinders in axial compression, *Composite Structures* 123 (2015) 190–203.
- [23] M. Rouhi, H. Ghayoor, S. V. Hoa, M. Hojjati, Computational efficiency and accuracy of multi-step design optimization method for variable stiffness composite structures, *Thin-Walled Structures* 113 (2017) 136–143.

ACCEPTED MANUSCRIPT